Low-Complexity Improved-Rate Generalised Spatial Modulation: Bit-to-Symbol Mapping, Detection and Performance Analysis

Jiancheng An, Chao Xu, *Senior Member, IEEE*, Yusha Liu,
Lu Gan, and Lajos Hanzo, *Life Fellow, IEEE*

Abstract—Low-complexity improved-rate generalised spatial modulation (LCIR-GSM) is proposed to mitigate the high complexity of the mapping book design and demodulation of variable-N_a GSM. Specifically, *first of all*, we propose two efficient schemes for mapping the information bits to the transmit antenna activation patterns, which can be readily scaled to massive MIMO setups. *Secondly*, we derive a pair of low-complexity near-optimal detectors, one of which has a reduced search scope, while the other benefits from a decoupled single-stream based signal detection algorithm. *Finally*, the performance of the proposed LCIR-GSM system is characterised by the improved error probability upper bound. Our simulation results confirm the improved error performance of our proposed scheme, despite its reduced signal detection complexity.

Index Terms—Generalised spatial modulation, maximum likelihood detection, bitwise spatial mapping, antenna selection.

I. INTRODUCTION

Spatial modulation (SM), constitutes a promising technique for the next-generation multiple-input multiple-output (MIMO) system, which has attracted substantial research interests [1]. More explicitly, for the SM scheme, the indices of the transmit antenna (TA) are exploited as an extra dimension for transmitting information besides the conventional amplitude-phase shift keying (APSK) symbols [2]. Since only a single TA is activated in SM-MIMO at any time instant, the inter-channel interference (ICI) and the inter-antenna interference (IAI) of conventional MIMO techniques are mitigated, which results in the simplified transceiver design and a reduced signal detection complexity [1], [2]. Specifically, the MIMO power consumption is effectively reduced since only a single power amplifier is required [3]. As a further advance, the SM scheme can be flexibly configured for challenging communication scenarios, such as the downlink MIMO systems having a rank-deficient channel matrix.

Inspired by the aforementioned advantages, the space shift keying concept was introduced in [4] as a low-complexity implementation of SM, where only the TA indices convey information. Furthermore, the principle of SM has also been extended to the time/frequency/code domain to exploit multiple degrees of freedom [5], [6]. As a result, the generalised

concept of index modulation has gained widespread interest in both academia and industry [7]–[9]. Besides, both the analytical studies, numerical simulation, as well as real-world experiments have verified that SM-MIMOs have the inherent potential of outperforming many state-of-art MIMO schemes, provided that a sufficiently high number of TAs are available at the transmitter [10].

In order to improve the achievable rate of single-RF SM schemes, generalised spatial modulation (GSM) was proposed upon activating multiple TAs simultaneously [11]. Furthermore, conventional full-RF diversity- and multiplexing-oriented MIMO schemes have been combined with GSM [12], [13] to achieve a beneficial diversity/multiplexing gain at the cost of using a reduced number of RF chains. Recently, the QSM mapping of [14] has been further improved in [15]–[17] by increasing the system's rate and/or reducing the bit error probability (BEP). However, all the aforementioned GSM-homologous schemes always employ a fixed number N_a of TAs, which inevitably results in the well-known rate limitation of the family of GSM schemes. In order to eliminate this rate limitation, the variable-N_a GSM (VGSM) concept was proposed for increasing the spatial constellation size by employing a variable number N_a of activated TAs [18], [19], which, however, results in high complexity of the mapping book design and demodulation.

Against this background, we present a low-complexity improved-rate generalised spatial modulation (LCIR-GSM) scheme. For the sake of illustration, features of the new LCIR-GSM scheme are compared to the existing GSM schemes in Table I. More explicitly, the contributions of the paper are as follows:

- Firstly, in order to alleviate the scalability problem of the existing VGSM codebook designs, we conceived three novel mapping arrangements, where the first two of which are proposed to mitigate the inherent problem of the so-called molecule shift keying (MoSK) scheme of [24] where no signal is transmitted for the special case of the all-zero bitstream. Furthermore, in order to maximize the Euclidean distance between spatial constellation points, the look-up table (LUT) arrangement of [18], [19] is further extended to our proposed scheme.
- Secondly, in order to mitigate the VGSM detection complexity, we propose a pair of low-complexity detectors based on the classical maximum likelihood detector (MLD). Explicitly, a two-step near-maximum likelihood detector (TMLD) is derived, which substantially narrows the search scope. Furthermore, a decoupling based maximum likelihood detector (DMLD) is conceived for decomposing a two-dimensional joint search into a pair of one-dimensional single-stream based searches, while still maintaining the optimal detection performance.
- Thirdly, we derive a tighter performance upper bound (UB) based on the framework of [27] for the proposed LCIR-GSM system. Explicitly, the improved performance bound reflects the impacts of the LCIR-GSM scheme's signal constellation diagram, spatial constellation diagram and their interactions, respectively. Finally, our simulation results confirm the improved spectral efficiency (SE),

TABLE I
THE CONTRIBUTION OF THE PROPOSED LCIR-GSM SCHEME COMPARED WITH OTHER GSM SCHEMES.

Contributions	LCIR-GSM	[20]	[21]	[22]	[9]	[15]	[23]	[24]	[18]	[12]	[25]	[26]
Flexibility in the number of TAs	✓	✓	×	✓	✓	✓	✓	✓	✓	✓	✓	✓
Multiple active TAs	✓	✓	×	✓	✓	✓	✓	✓	✓	✓	✓	✓
Multiple streams	×	✓	×	✓	✓	✓	✓	×	×	✓	×	✓
Variable number of active TAs	✓	×	×	×	×	×	×	✓	✓	×	✓	×
Improved bitwise spatial mapping	✓	×	×	×	×	×	×	×	×	×	×	×
Joint spatial and classic symbol alphabet	✓	✓	✓	×	✓	×	✓	×	×	✓	×	×
Low-complexity detectors	✓	✓	×	×	×	×	×	×	×	✓	×	×
Improved upper bound	✓	×	✓	×	×	×	×	×	×	×	×	×

reduced signal detection complexity and improved BEP performance of our proposed LCIR-GSM scheme.

The rest of this paper is structured as follows. Sec. II presents the LCIR-GSM system model and spatial mapping schemes. Our detection algorithms are conceived in Sec. III. Sec. IV analyses the theoretical BEP and computational complexity of the LCIR-GSM system, while the BEP performance of our LCIR-GSM systems is presented in Sec. V. Finally, Sec. VI concludes the paper.

II. SYSTEM MODEL

A. LCIR-GSM Transmission

In LCIR-GSM systems, the incoming data bits are first grouped per $m = m_s + m_a$ bits. Following this, the grouped block of bits $\mathbf{b}^T$ is split into m_s spatial bits $\mathbf{b}_s^T$ and m_a APSK modulated symbol bits $\mathbf{b}_a^T$, i.e., $\mathbf{b}^T = \left[\mathbf{b}_s^T \middle| \mathbf{b}_a^T \right]$. The first m_s spatial bits are assigned to select the TA activation pattern following the spatial mapping procedures. The remaining m_a bits are modulated using M-APSK with the modulation order of $M = 2^{m_a}$. In contrast to the classic GSM, which activates a fixed number of TAs at each slot, the number of activated TAs in the LCIR-GSM scheme is variable [18], [19] for the sake of utilizing all legitimate TA activation patterns. The total number N_m of all legitimate TA activation patterns is given by $N_m = C_{N_t}^0 + C_{N_t}^1 + \cdots + C_{N_t}^{N_t} = 2^{N_t}$, where $C_{N_t}^0$ corresponds to the spatial bit sequence having all zeros. Assuming that the case of $\mathbf{b}_s^T = \mathbf{0}$ is disabled, the maximum value of m_s becomes[1] $m_s = \lfloor \log (N_m - 1) \rfloor = \lfloor \log (2^{N_t} - 1) \rfloor = N_t - 1$. In summary, the total number of source bits conveyed by the LCIR-GSM design is given by $m = m_a + m_s = \log M + N_t - 1$, which is evidently higher than that of GSM given by $\log M + \lfloor \log C_{N_t}^{N_a} \rfloor$, where N_a is the number of RF chains.

In the LCIR-GSM system, the transmit signal $\mathbf{x} \in \mathbb{C}^{N_t \times 1}$ is transmitted over an $N_t \times N_r$ MIMO Rayleigh flat fading wireless channel, $\mathbf{H} = [\mathbf{h}_1 \cdots \mathbf{h}_{N_t}]$. The entries of $\mathbf{H}$ are generated by i.i.d. complex Gaussian random variables having zero-mean and unit-variance. As a result, the signal $\mathbf{y}$ received at any instant is given by

$$\mathbf{y} = \mathbf{H}\mathbf{x} + \mathbf{n} = \mathbf{h}_{\mathcal{S}_k} s + \mathbf{n}, \tag{1}$$

where $s \in M$-APSK is the modulated symbol, while $\mathcal{S}_k$ is the k-th TA activation combination associated with $k \in \{1, \cdots, 2^{N_t-1}\}$. The mapping mechanism of $\{\mathcal{S}_1, \cdots, \mathcal{S}_{2^{N_t-1}}\}$

[1] We note that m_s is increased beyond this rate limit by the first of our spatial mapping schemes proposed in Sec. II-B, namely in DTAA-R, where we have $m_s = \log (2^{N_t}) = N_t$.

will be detailed in Sec. II-B. Furthermore, the channel vector can be expressed as $\mathbf{h}_{\mathcal{S}_k} = \sum_{k \in \mathcal{S}_k} \mathbf{h}_k$, which is the summation of all channel vectors corresponding to the k-th TA activation patterns. Moreover, $\mathbf{n}$ is an AWGN vector associated with zero-mean and variance of σ_n^2 in each dimension.

B. LCIR-GSM spatial mapping scheme

Next, we introduce three spatial mapping arrangements for LCIR-GSM systems, which are: 1) direct TA activation relying on constellation rotation (DTAA-R), 2) direct TA activation relying on a dedicated TA (DTAA-D) and 3) LUT. More specifically, DTAA-R and DTAA-D are the improved schemes of the bitwise activation scheme of the MoSK [24], while LUT uses the same mapping design as VGSM of [18], [19], which we include aims to share the low-complexity detectors proposed in Sec. III.

1) DTAA-R: The motivation of the DTAA-R scheme is to establish a direct mapping between the spatial bits and the TA activation pattern, which does not require a large LUT. The simplest way is to assign each spatial bit to independently control the ON/OFF state of the TAs. However, as mentioned before, when all spatial bits of $\mathbf{b}_s$ are zeros, no TAs are activated to transmit the classic M-PSK/QAM symbol, which constitutes a challenge in our DTAA-R design. In order to solve this problem, we propose the following revised DTAA-R mapping rule:

$$\begin{cases} \mathbf{b}_s^T \neq \mathbf{0} \Leftrightarrow \mathbf{x} = \mathbf{b}_s \times s \\ \mathbf{b}_s^T = \mathbf{0} \Leftrightarrow \mathbf{x} = \mathbf{1} \times T(s), \end{cases} \tag{2}$$

where $\mathbf{1}$ is a $N_t \times 1$ column vector of ones. In this way, all TAs are activated, when the spatial bits are all zeros. Moreover, since the TA activation pattern corresponding to $\mathbf{b}_s^T = \mathbf{0}$ becomes exactly the same as in the case of $\mathbf{b}_s^T = \mathbf{1}$, we propose to apply a transformation $T(\cdot)$ to the APSK constellation. Explicitly, for an M-PSK symbol, a simple phase rotation is applied to the APSK symbol, when all the TAs are activated for $\mathbf{b}_s^T = \mathbf{0}$, which can be expressed as: $T_{PSK}(s) = e^{j \frac{\pi}{M}} s$. By contrast, when M-QAM is employed instead of M-PSK, the above phase rotation no longer maximises the distance in the constellation. Instead, we propose the following transformation: $T_{QAM}(s) = e^{j \frac{\pi}{M_n}} s$, where M_n represents the mode of the QAM amplitude set. For example, we have $M_n = 8$ and $M_n = 12$ for normalised 16QAM and 64QAM constellation, respectively.

2) DTAA-D: Instead of implementing a phase rotation to the APSK constellation, in this section, we propose the DTAA-D mapping method, which assigns a dedicated TA to be uniquely turned on only for the all-zero spatial bitstream. As a result, the ON/OFF states of the $(N_t - 1)$ TAs are decided by the

$(N_t - 1)$ non-all-zero spatial bits without any ambiguity, hence eliminating the dependence of the DTAA-R scheme on the constellation rotation. More explicitly, the DTAA-D mapping rule is defined by

$$\begin{cases} \mathbf{b}_s^T \neq \mathbf{0} \Leftrightarrow \mathbf{x} = \begin{bmatrix} \mathbf{b}_s^T & 0 \end{bmatrix}^T \times s \\ \mathbf{b}_s^T = \mathbf{0} \Leftrightarrow \mathbf{x} = \begin{bmatrix} \mathbf{0}_{(N_t-1)\times 1}^T & 1 \end{bmatrix}^T \times s. \end{cases} \quad (3)$$

where the last TA is activated for the special case of $\mathbf{b}_s^T = \mathbf{0}$.

3) LUT: The DTAA-D arrangement is capable of achieving the full LCIR-GSM rate without any constellation rotation, but unfortunately, the distance between the legitimate TA activation patterns has not been maximised. Against this background, the LUT arrangement is introduced to further optimize the DTAA-D scheme's spatial constellation, but suffer from the high complexity of the mapping design [18], [19]. In summary, the LUT arrangement is exemplified by:

$$\mathbf{b}_s^T \Leftrightarrow \mathbf{x} = \mathrm{U}(\mathbf{b}_s) \times s, \quad (4)$$

where $\mathrm{U}(\cdot)$ returns a column vector having entries of 0 or 1, thus ensuring that the binary vectors $\{\mathrm{U}(\mathbf{b}_s)\}_{\forall \mathbf{b}_s}$ have the maximum possible Hamming distance [18], [19].

III. SIGNAL DETECTION

In this section, we proceed to devise low-complexity signal detectors for the LCIR-GSM receiver. We first consider the optimal MLD in Sec. III-A, followed by a pair of reduced-complexity detectors in Sec. III-B and III-C, respectively.

A. Maximum Likelihood Detection

From the detector's perspective, let us represent the tentative transmitted signal vector as $\mathbf{x}_{k,l}$ with k denoting the k-th TA activation pattern and l denoting the l-th M-APSK symbol. We assume that perfect CSI is available at the receiver. As a result, the MLD finds the estimate of $\mathbf{x}$ by performing a full search over all legitimate indices k and l formulated as [28]:

$$[\hat{k}_{MLD}, \hat{l}_{MLD}] = \arg\min_{k,l} \|\mathbf{y} - \mathbf{g}_k s_l\|^2, \quad (5)$$

where s_l represents the l-th symbol of the constellation, and $\mathbf{g}_k$ is the k-th column of the equivalent $N \times N_r$ LCIR-GSM channel matrix $\mathbf{G}$, where we have $N = 2^{N_t}$ for DTAA-R and $N = 2^{N_t-1}$ for DTAA-D and LUT. In summary, the equivalent channel matrix $\mathbf{G}$ is defined as follows

$$\begin{cases} \mathbf{G}_{DTAA-R} = \begin{bmatrix} \mathbf{Hb}_{s,1} & \cdots & \mathbf{Hb}_{s,N-1} & \mathbf{H1}e^{j\frac{\pi}{M_n}} \end{bmatrix} \\ \mathbf{G}_{DTAA-D} = \begin{bmatrix} \mathbf{H}\begin{bmatrix} \mathbf{b}_{s,1} \\ 0 \end{bmatrix} & \cdots & \mathbf{H}\begin{bmatrix} \mathbf{b}_{s,N-1} \\ 0 \end{bmatrix} & \mathbf{H}\begin{bmatrix} \mathbf{0} \\ 1 \end{bmatrix} \end{bmatrix} \\ \mathbf{G}_{LUT} = \begin{bmatrix} \mathbf{HU}(\mathbf{b}_{s,0}) & \mathbf{HU}(\mathbf{b}_{s,1}) & \cdots & \mathbf{HU}(\mathbf{b}_{s,N-1}) \end{bmatrix}, \end{cases} \quad (6)$$

where $M_n = M$ for M-PSK, and $\mathbf{b}_{s,0} = \mathbf{0}$ denotes the spatial bitstream with all zeros. Observe seen from (5) that the LCIR-GSM system is now equivalent to an SM system with N TAs, where all of the three mapping arrangements share the same detector structure.

B. Two-stage near-Maximum Likelihood Detection

The MLD has to jointly search through N TA activation patterns and M symbols, hence its complexity order is given by $O(MN)$, which grows exponentially both with the number N_t of TAs and number m_s of modulated bits. In this section, we conceive the low-complexity TMLD scheme, which follows a similar philosophy to the sphere decoder of [29]. This two-stage TMLD first detects the modulated symbol index l from the reduced search space as follows:

$$\hat{l} = \arg\min_l \|\mathbf{y} - \mathbf{h}_{k'}s_l\|^2. \quad (7)$$

We note that the range of k' is given by $k' \in \{1, 2, \cdots, N_t\}$, which is reduced from $k \in \{1, 2, \cdots, N\}$.

Then, the TMLD relaxes the range of l appropriately based on the estimated $\hat{l}$, which means several l values can be selected based on (7), instead of a single $\hat{l}$, since a single one would unlikely to be the globally optimal one. Therefore, TMLD defines the reduced candidate set of l using $\hat{l}$ in (7) as $\chi_{TMLD} = \left\{ l \mid \|\mathbf{y} - \mathbf{h}_{k'}s_l\|^2 \leq c\|\mathbf{y} - \mathbf{h}_{k'}s_{\hat{l}}\|^2 \right\}$, where $c \geq 1$ is a constant controlling the cardinality of χ_{TMLD}.

Following this, the second stage of TMLD is performed based on (5) as:

$$[\hat{k}_{TMLD}, \hat{l}_{TMLD}] = \arg\min_{k,l \in \chi_{TMLD}} \|\mathbf{y} - \mathbf{g}_k s_l\|^2. \quad (8)$$

The MLD guarantees that the solution is optimal by searching through all the elements in the available set. By contrast, TMLD searches for k and l in a reduced region by relaxing the rough estimate of l, which is similar to the sphere decoding philosophy of [29]. As c goes to infinity, TMLD becomes equivalent to MLD.

C. Decoupling Based Maximum Likelihood Detection

In this subsection, we propose the novel DMLD, which firstly obtains the optimum modulation indices for all TA activation pattern candidates and then detects the optimal TA activation pattern with the aid of the demodulated M-APSK symbol. More explicitly, for each tentative TA combination index k, the LCIR-GSM detection in (5) can be simplified to

$$\hat{l}_k = \arg\min_l \left\{ |s_l - p_k|^2 \right\}, \quad (9)$$

where the demodulator's decision variable is given by $p_k = \mathbf{g}_k^H \mathbf{y} / \|\mathbf{g}_k\|^2$ [30]. In this way, the optimum modulated symbol index $\hat{l}_k$ associated with all TA activation indices may be directly obtained by demapping p_k to the closest constellation point, assuming that a regular APSK constellation is used.

When M-PSK is employed, the demodulation of (9) may be performed by rounding the phase of the decision variable to the nearest M-PSK index as [30]

$$\hat{s}_k = \exp\left\{ j\left[\frac{\pi}{2}\left\lfloor (\angle p_k - \phi_0)\frac{2}{\pi} \right\rceil + \phi_0 \right] \right\}, \quad (10)$$

where ϕ_0 is the phase of the first M-PSK symbol associated with all-zero bits. Similarly, the QAM slicing can be performed as shown in [31], which is omitted here for the sake of brevity.

Thus we obtain the total number N of demodulated symbols $S_{min} = \{\hat{s}_1, \cdots, \hat{s}_N\}$ associated with the N hypotheses. As a result, we have

$$\hat{k}_{DMLD} = \arg\min_k \|\mathbf{y} - \mathbf{g}_k \hat{s}_k\|^2. \quad (11)$$

Once $\hat{k}_{DMLD}$ is estimated, we have $\hat{s}_{DMLD} = \hat{s}_{\hat{k}_{DMLD}}$, which is the $\hat{k}_{DMLD}$-th element of S_{min}.

The DMLD's complexity order does not grow with the modulation levels, which constitutes the most appealing benefits, especially for high-order M-PSK/QAM schemes.

IV. Performance Analysis

In this section, we present analytical results for characterising the error performance of the uncoded LCIR-GSM system, where the MLD is assumed to obtain the optimal reference bound. A tight UB on the BEP is derived. Additionally, we also discuss the computational complexity of the proposed LCIR-GSM detectors.

A. Uncoded Error Performance

1) Classic Union Bound: First of all, the analytical performance of our LCIR-GSM system is evaluated using the well-known union bounding technique. More specifically, the average BEP of LCIR-GSM is given by: [28]

$$P_b \leq \frac{1}{MN} \sum_{k,\tilde{k}} \sum_{l,\tilde{l}} N_{\mathbf{x}_{k,l} \to \mathbf{x}_{\tilde{k},\tilde{l}}} \mu_\alpha^{N_r} \sum_{n=0}^{N_r-1} C_{N_r-1+n}^n (1-\mu_\alpha)^n, \quad (12)$$

with $\mu_\alpha = \frac{1}{2}\left(1 - \sqrt{\frac{\sigma_\alpha^2}{1+\sigma_\alpha^2}}\right)$ and $\sigma_\alpha^2 = \frac{1}{4\sigma_n^2}\left(|s_l|^2 + |s_{\tilde{l}}|^2\right)$.

2) Improved Upper Bound: The theoretical UB above is derived based on the conventional SM study of [28], which does not take into account the specific effects of the spatial constellation and symbol constellation. To avoid these limitations, an improved UB paradigm is proposed in [27], based on which we derive our improved performance bound for LCIR-GSM. Specifically, *Proposition 1* gives the improved UB of our LCIR-GSM system under Rayleigh flat fading.

Proposition 1: The average BEP of LCIR-GSM can be tightly upper bounded as follows:

$$P_b \leq P_{b,signal} + P_{b,spatial} + P_{b,joint}, \quad (13)$$

where $P_{b,signal}$, $P_{b,spatial}$, $P_{b,joint}$ are defined as the similar form in [27].

As shown in *Proposition 1* of [27], in order to obtain the ABEP upper bound characterized by (13), the moment generating functions of $\gamma\left(\mathbf{b}_{s,k}, \mathbf{b}_{s,\tilde{k}}\right)$ and $\gamma\left(\mathbf{x}_{k,l}, \mathbf{x}_{\tilde{k},\tilde{l}}\right)$ have to be derived for our proposed GSM design. According to [19], we have:

$$\gamma\left(\mathbf{b}_{s,k}, \mathbf{b}_{s,\tilde{k}}\right) = \breve{\mathbf{g}}^T \left[\mathbf{I}_N \otimes (\mathbf{e}_k - \mathbf{e}_{\tilde{k}})(\mathbf{e}_k - \mathbf{e}_{\tilde{k}})^H\right] \breve{\mathbf{g}}^*, \quad (14)$$

$$\gamma\left(\mathbf{x}_{k,l}, \mathbf{x}_{\tilde{k},\tilde{l}}\right) = \breve{\mathbf{g}}^T \left[\mathbf{I}_N \otimes \left(\mathbf{x}_{k,l} - \mathbf{x}_{\tilde{k},\tilde{l}}\right)\left(\mathbf{x}_{k,l} - \mathbf{x}_{\tilde{k},\tilde{l}}\right)^H\right] \breve{\mathbf{g}}^*, \quad (15)$$

where $\mathbf{e}_k$ is the $N_t \times 1$ unit vector associated with only the k-th entry of 1, and $\breve{\mathbf{g}} = \text{vec}\left(\mathbf{G}^T\right)$ is a $N_r N \times 1$ vector obtained by the vectorization of $\mathbf{G}^T$. Although the canonical i.i.d. Rayleigh fading scenario is investigated, the equivalent LCIR-GSM channels are correlated. In light of this, the MGFs of $\gamma\left(\mathbf{b}_{s,k}, \mathbf{b}_{s,\tilde{k}}\right)$ and $\gamma\left(\mathbf{x}_{k,l}, \mathbf{x}_{\tilde{k},\tilde{l}}\right)$ are derived based on the methodology of [19] as

$$M_{\gamma\left(\mathbf{b}_{s,k}, \mathbf{b}_{s,\tilde{k}}\right)}(t) = \det\left[\mathbf{I}_{N_r N} + t\mathbf{C}_{\breve{\mathbf{g}}}\left(\mathbf{I}_N \otimes \left(\mathbf{u}\mathbf{u}^H\right)\right)\right]^{-1}, \quad (16)$$

$$M_{\gamma\left(\mathbf{x}_{k,l}, \mathbf{x}_{\tilde{k},\tilde{l}}\right)}(t) = \det\left[\mathbf{I}_{N_r N} + t\mathbf{C}_{\breve{\mathbf{g}}}\left(\mathbf{I}_N \otimes \left(\mathbf{v}\mathbf{v}^H\right)\right)\right]^{-1}, \quad (17)$$

where we have $\mathbf{u} = \mathbf{e}_k - \mathbf{e}_{\tilde{k}}$ and $\mathbf{v} = \mathbf{x}_{k,l} - \mathbf{x}_{\tilde{k},\tilde{l}}$, while $\det(\mathbf{S})$ denotes the determinant of the matrix $\mathbf{S}$. Furthermore, $\mathbf{C}_{\breve{\mathbf{g}}} = \frac{1}{N_r}\mathbf{I}_{N_r} \otimes \mathbb{E}\left(\mathbf{G}^T \mathbf{G}^*\right)$ is the covariance matrix of $\breve{\mathbf{g}}$, which is determined by the particular spatial mapping scheme

introduced in Sec. II-B. More specifically, the $(k, \tilde{k})$ element of $\mathbf{C}_{\mathbf{G}^T} = \frac{1}{N_r}\mathbb{E}\left(\mathbf{G}^T \mathbf{G}^*\right)$ is equal to the number of activated TAs shared by the k-th and $\tilde{k}$-th TA activation patterns. After substituting (16) and (17) into (7) $\sim$ (8) of [19], we arrive at $P_{b,spatial}$ and $P_{b,joint}$, respectively. Interested readers might like to refer to our full manuscript [32] for the closed-form expression, which is omitted here for the sake of brevity. We note that the numerical integrals therein can be further simplified upon leveraging the Chernoff bound [19].

On the other hand, $P_{b,signal}$ can be further simplified to

$$P_{b,signal} = \frac{\log M}{\log(MN)} P_{b,MOD}^{Rayleigh}, \quad (18)$$

where $P_{b,MOD}^{Rayleigh}$ can be obtained following the steps in [33] for PSK and QAM constellations, respectively.

The theoretical analysis provides useful insights into the performance of LCIR-GSM systems. For example, it shows that the bit mapping of the PSK/QAM constellation diagram plays an important role in $P_{b,joint}$. In particular, while conventional bit mappings based on the Euclidean distance of the signal constellations turn out to be optimal for minimising $P_{b,signal}$, additional constraints may be imposed onto the best choice of the signal constellation diagram and onto the related bit mapping for minimising $P_{b,signal}$ and $P_{b,joint}$ simultaneously.

B. Complexity Analysis

In this part, we compare the computational complexity of the detectors proposed for our LCIR-GSM scheme. The detection complexity is quantified in terms of the number of real-valued multiplications required. The complexity of GSM in [11] is given by $\delta_{GSM} = 6MN_r 2^{\lfloor \log C_{N_t}^{N_a} \rfloor}$. Similarly, for the proposed LCIR-GSM scheme, the detection complexity of the full-search based MLD of (5) is given by

$$\delta_{MLD} = 6MN_r N, \quad (19)$$

since one complex-valued multiplication and modulo square operations are carried out for each dimension.

Following the same philosophy, when the near-optimal reduced-scope TMLD of (8) is used, the LCIR-GSM scheme's complexity becomes

$$\delta_{TMLD} = 6MN_r N_t + 6\beta MN_r N, \quad (20)$$

where $\frac{1}{M} \leq \beta \leq 1$ is a parameter that increases with the constant c. More specifically, we have $\beta = \frac{1}{M}$ for $c = 1$ and $\beta \to 1$ for $c \to \infty$, respectively. We note that as $c \to \infty$, the complexity of TMLD becomes higher than that of MLD, which is because TMLD does not reduce the cardinality of the symbol constellation for a large c, but increases the complexity of the first step. However, in practice, a small value of c is adequate for achieving near-ML performance at a low complexity.

When the single-stream-based DMLD of (9)-(11) is invoked, the LCIR-GSM detection complexity encountered for a given k consists of three parts: 1) the computation of p_k in (9) requires $(6N_r + 2)$ real-valued multiplications [31]; 2) 2 and 4 real-valued multiplications are required for obtaining $\hat{s}_k$ in PSK and QAM, respectively; 3) 6 real-valued multiplications are required for performing (11). Therefore, the LCIR-GSM detection complexity is reduced to

$$\delta_{DMLD} = \begin{cases} (6N_r + 10)N, & PSK \\ (6N_r + 12)N, & QAM \end{cases}, \quad (21)$$
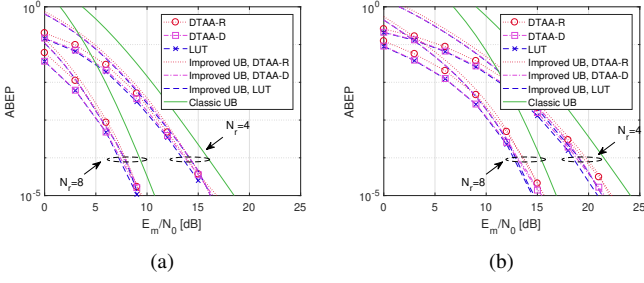
Fig. 1. ABEP of LCIR-GSM ($N_t = 6$) versus E_m/N_0 under our three types of spatial mapping rules. (a) QPSK; (b) 16QAM.
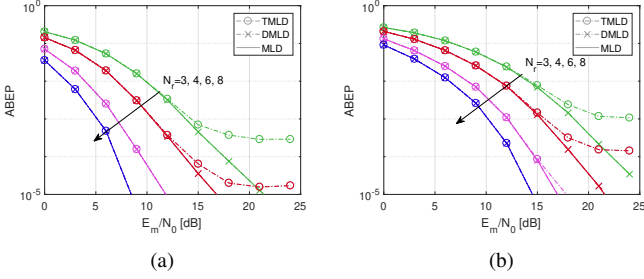

Fig. 2. ABEP of LCIR-GSM ($N_t = 6$) versus E_m/N_0 for our three types of detectors. The LUT is used to illustrate the compatibility of the proposed low-complexity detectors. (a) QPSK; (b) 16QAM.

Fig. 3. The performance comparison between LCIR-GSM (QPSK) and GSM for different N_a. (a) $N_t = 5$ is used to maintain an overall rate of 6bpcu; (b) $N_t = 6$ is used to maintain an overall rate of 7bpcu.

Fig. 4. Complexity comparison of different detectors for LCIR-GSM with $N_r = 6$, where DTAA-D and LUT are adopted.

V. SIMULATION RESULTS

In this section, the BEP performance of LCIR-GSM systems is investigated for different numbers of TA/RAs and using different modulation schemes. For the sake of clarity, the parameters used for generating the results in this section are detailed in the figures. Please bear in mind that the LUT-based scheme actually represents the existing VGSM scheme of [18].

Fig. 1 contrast our simulations and theoretical derivations for the LCIR-GSM system, where the MLD is adopted. Although the three mapping arrangements only exhibit modest performance differences in Fig. 1, the DTAA-R is shown to have a worse BEP than DTAA-D and LUT, since it transmits one more bit using the same number of TAs. By contrast, the LUT performs the best, which, however, has to rely on a pre-defined codebook thus imposing a higher design complexity. Moreover, it is demonstrated that the improved theoretical bound is about 1.5dB tighter than the conventional bound. Furthermore, as the number of RAs increases, the performance advantage of LUT over DTAA-R/DTAA-D improves, and the UB also becomes tighter.

Fig. 2 compares the performance of different detectors for our LCIR-GSM system having $N_t = 6$. As discussed in Sec. IV-B, the TMLD exhibits a lower detection complexity, but it also imposes a performance loss compared to the MLD and DMLD, as confirmed by Fig. 2. We note that the constant c in TMLD is set to 1.5 in Fig. 2, which may be increased for improving the performance but resulting in a higher detection complexity. Moreover, Fig. 2 shows that TMLD suffers from an error floor, which moves down upon increasing N_r because
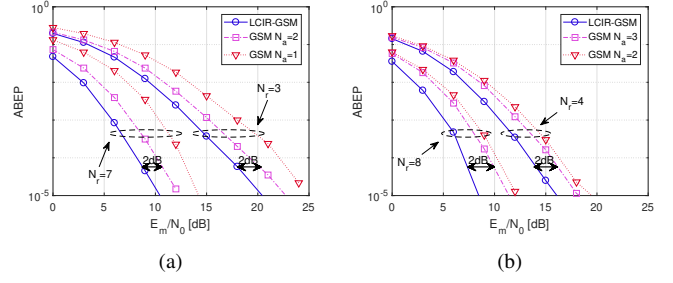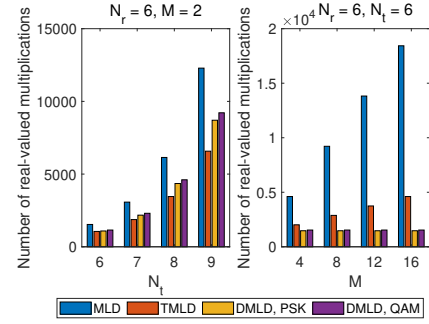
the channels between different TAs tend to become more orthogonal for an increased number of RAs. Hence the index of the modulated symbol found in the first step becomes more accurate. Fortunately, DMLD always maintains the same performance as MLD, which benefits from the fact that for a regular constellation, the rounding-based detector and the exhaustive search return the same result.

The BEP performance comparisons between GSM and LCIR-GSM are offered in Fig. 3. In Fig. 3(a), the number of TAs is set to $N_t = 5$ and QPSK is used for LCIR-GSM. In order to maintain the overall rate of 6bpcu, 16QAM and 8QAM are used for GSM with the fixed number of active TAs $N_a = 1$ and $N_a = 2$, respectively. It can be seen in Fig. 3(a) that LCIR-GSM outperforms GSM for $N_a = 2$ by about 2dB for different numbers of RAs. When GSM associated with $N_a = 1$ is considered, a 4dB performance gain can be observed in Fig. 3(a). Fig. 3(b) portrays the performance comparisons between GSM and LCIR-GSM for the case of $N_t = 6$. The QPSK constellation is also adopted for LCIR-GSM, while 16QAM and 8QAM are used for GSM at $N_a = 2$ and $N_a = 3$, respectively, hence maintaining an overall rate of 7bpcu. The 2dB performance gain compared to GSM using $N_a = 3$ can also be observed in Fig. 3(b) to verify the advantage of the proposed LCIR-GSM scheme.

Finally, Fig. 4 compares the computational complexity of different detectors, where we set $c = 1$ for TMLD. As seen in Sec. IV-B, the complexity of MLD is prohibitive and increases exponentially with N_t, while our proposed detectors achieve lower complexity for all the scenarios considered. Specifically, the TMLD's complexity is lower than DMLD for a small

constellation, and the complexity difference will widen as the number of TAs increases. By contrast, for a moderate number of TAs, the DMLD is more competitive in conjunction with high-order modulation, which is because the complexity of the DMLD does not increase with the constellation size M. In summary, the proposed low-complexity TMLD detector strikes an attractive BEP performance vs. detection complexity tradeoff and can be applied flexibly in various scenarios. Moreover, we emphasize that the DMLD is always optimal but it is only suitable for regular constellations, while the TMLD is suboptimal.

VI. CONCLUSIONS

A novel LCIR-GSM scheme was proposed in order to improve the GSM mapping mechanism and reduce the detection complexity. More specifically, for the LCIR-GSM mapping, the DTAA-R, DTAA-D and LUT arrangements are conceived to facilitate a flexible MIMO deployment, with special attention dedicated to the all-zero spatial beam stream. Furthermore, as for the LCIR-GSM signal detection, we have developed the low-complexity TMLD and DMLD approaches, where the former adopts the sphere decoding philosophy for the sake of striking a compelling performance vs complexity trade-off. By contrast, the latter is capable of achieving the ML performance at a single-stream detection complexity that does not escalate with the number of modulation levels. Furthermore, an improved theoretical UB is derived for the proposed LCIR-GSM, which is confirmed by our simulations to be about 1.5dB tighter than the existing conventional solution. Finally, our simulation results demonstrate that the proposed LCIR-GSM scheme achieves improved performance over the conventional GSM, despite its lower complexity than that of VGSM.

REFERENCES

[1] R. Y. Mesleh, H. Haas, S. Sinanovic, C. W. Ahn, and S. Yun, "Spatial modulation," *IEEE Trans. Veh. Technol.*, vol. 57, no. 4, pp. 2228–2241, 2008.

[2] M. Di Renzo, H. Haas, A. Ghrayeb, S. Sugiura, and L. Hanzo, "Spatial modulation for generalized MIMO: Challenges, opportunities, and implementation," *Proc. IEEE*, vol. 102, no. 1, pp. 56–103, 2013.

[3] C. Masouros and L. Hanzo, "Constellation randomization achieves transmit diversity for single-RF spatial modulation," *IEEE Trans. Veh. Technol.*, vol. 65, no. 10, pp. 8101–8111, 2015.

[4] J. Jeganathan, A. Ghrayeb, L. Szczecinski, and A. Ceron, "Space shift keying modulation for MIMO channels," *IEEE Trans. Wireless Commun.*, vol. 8, no. 7, pp. 3692–3703, 2009.

[5] S. Sugiura, S. Chen, and L. Hanzo, "Coherent and differential space-time shift keying: A dispersion matrix approach," *IEEE Trans. Commun.*, vol. 58, no. 11, pp. 3219–3230, 2010.

[6] H. A. Ngo and L. Hanzo, "Area spectral efficiency of soft-decision space–time–frequency shift-keying-aided slow-frequency-hopping multiple access," *IEEE Trans. Veh. Technol.*, vol. 61, no. 3, pp. 1433–1439, 2012.

[7] E. Basar, "Index modulation techniques for 5G wireless networks," *IEEE Commun. Mag.*, vol. 54, no. 7, pp. 168–175, 2016.

[8] T. Mao, Q. Wang, Z. Wang, and S. Chen, "Novel index modulation techniques: A survey," *IEEE Commun. Surveys Tuts.*, vol. 21, no. 1, pp. 315–348, 2018.

[9] M. Al-Nahhal, E. Basar, and M. Uysal, "Flexible generalized spatial modulation for visible light communications," *IEEE Trans. Veh. Technol.*, vol. 70, no. 1, pp. 1041–1045, 2021.

[10] N. Serafimovski, A. Younis, R. Mesleh, P. Chambers, M. Di Renzo, C.-X. Wang, P. M. Grant, M. A. Beach, and H. Haas, "Practical implementation of spatial modulation," *IEEE Trans. Veh. Technol.*, vol. 62, no. 9, pp. 4511–4523, 2013.

[11] A. Younis, N. Serafimovski, R. Mesleh, and H. Haas, "Generalised spatial modulation," in *Proc. IEEE Asilomar Conf. Signals Syst. Comput.* IEEE, 2010, pp. 1498–1502.

[12] J. Wang, S. Jia, and J. Song, "Generalised spatial modulation system with multiple active transmit antennas and low complexity detection scheme," *IEEE Trans. Wireless Commun.*, vol. 11, no. 4, pp. 1605–1615, 2012.

[13] T. Datta, H. S. Eshwaraiah, and A. Chockalingam, "Generalized space-and-frequency index modulation," *IEEE Trans. Veh. Technol.*, vol. 65, no. 7, pp. 4911–4924, 2015.

[14] R. Mesleh, S. S. Ikki, and H. M. Aggoune, "Quadrature spatial modulation," *IEEE Trans. Veh. Technol.*, vol. 64, no. 6, pp. 2738–2742, 2014.

[15] L. Xiao, P. Xiao, Y. Xiao, H. Haas, A. Mohamed, and L. Hanzo, "Compressive sensing assisted generalized quadrature spatial modulation for massive MIMO systems," *IEEE Trans. Commun.*, 2019.

[16] M. Mohaisen, "Increasing the minimum euclidean distance of the complex quadrature spatial modulation," *IET Commun.*, vol. 12, no. 7, pp. 854–860, 2018.

[17] R. Mesleh, O. Hiari, and A. Younis, "Generalized space modulation techniques: Hardware design and considerations," *Physical Commun.*, vol. 26, pp. 87–95, 2018.

[18] O. Osman, "Variable active antenna spatial modulation," *IET Microw., Antennas Propag.*, vol. 9, no. 15, pp. 1816–1824, 2015.

[19] A. Younis, "Spatial modulation: Theory to practice," *Ph.D. dissertation*, Instit. Digit. Commun., School Eng., Univ. Edinburgh, Edinburgh, Scotland, 2014.

[20] L. Xiao, Y. Xiao, L. You, P. Yang, S. Li, and L. Hanzo, "Single-RF and Twin-RF spatial modulation for an arbitrary number of transmit antennas," *IEEE Trans. Veh. Technol.*, vol. 67, no. 7, pp. 6311–6324, 2018.

[21] P. S. Koundinya, K. Hari, and L. Hanzo, "Joint design of the spatial and of the classic symbol alphabet improves single-RF spatial modulation," *IEEE Access*, vol. 4, pp. 10 246–10 257, 2016.

[22] L. He, J. Wang, and J. Song, "Spatial modulation for more spatial multiplexing: RF-chain-limited generalized spatial modulation aided mm-wave MIMO with hybrid precoding," *IEEE Trans. Commun.*, vol. 66, no. 3, pp. 986–998, 2017.

[23] S. Guo, H. Zhang, P. Zhang, S. Dang, L. Cong, and M.-S. Alouini, "Signal shaping for generalized spatial modulation and generalized quadrature spatial modulation," *arXiv preprint arXiv:1901.09318*, 2019.

[24] M. H. Kabir, S. R. Islam, and K. S. Kwak, "D-MoSK modulation in molecular communications," *IEEE Trans. Nanobiosci.*, vol. 14, no. 6, pp. 680–683, 2015.

[25] P. Liu, M. Di Renzo, and A. Springer, "Variable-N_u generalized spatial modulation for indoor los mmwave communication: Performance optimization and novel switching structure," *IEEE Trans. Commun.*, vol. 65, no. 6, pp. 2625–2640, 2017.

[26] G. Xia, Y. Lin, X. Zhou, W. Zhang, F. Shu, and J. Wang, "Hybrid precoding design for secure generalized spatial modulation with finite-alphabet inputs," *IEEE Trans. Commun.*, vol. 69, no. 4, pp. 2570–2584, 2021.

[27] M. Di Renzo and H. Haas, "Bit error probability of SM-MIMO over generalized fading channels," *IEEE Trans. Veh. Technol.*, vol. 61, no. 3, pp. 1124–1144, 2012.

[28] J. Jeganathan, A. Ghrayeb, and L. Szczecinski, "Spatial modulation: Optimal detection and performance analysis." *IEEE Commun. Lett.*, vol. 12, no. 8, pp. 545–547, 2008.

[29] A. Younis, S. Sinanovic, M. Di Renzo, R. Mesleh, and H. Haas, "Generalised sphere decoding for spatial modulation," *IEEE Trans. Commun.*, vol. 61, no. 7, pp. 2805–2815, 2013.

[30] C. Xu, S. Sugiura, S. X. Ng, P. Zhang, L. Wang, and L. Hanzo, "Two decades of MIMO design tradeoffs and reduced-complexity MIMO detection in near-capacity systems," *IEEE Access*, vol. 5, pp. 18 564–18 632, 2017.

[31] R. Rajashekar, K. Hari, and L. Hanzo, "Reduced-complexity ML detection and capacity-optimized training for spatial modulation systems," *IEEE Trans. Commun.*, vol. 62, no. 1, pp. 112–125, 2013.

[32] J. An, C. Xu, Y. Liu, L. Gan, and L. Hanzo, "Low-complexity improved-throughput generalised spatial modulation: Bit-to-symbol mapping, detection and performance analysis," Jul. 2021, [Online]. Available: https://arxiv.org/abs/2107.12630.

[33] M. K. Simon and M.-S. Alouini, *Digital communication over fading channels.* John Wiley & Sons, 2005.